Journal of Molecular Liquids 243 (2017) 439–450

Contents lists available at ScienceDirect

Journal of Molecular Liquids

journal homepage: www.elsevier.com/locate/molliq

Corrosion inhibition performance of chromone-3-acrylic acid derivatives for low alloy steel with theoretical modeling and experimental aspects

Rajeev Kumar [a], Savita Chahal [a], Sumit Kumar [a], Suman Lata [a,*], Hassane Lgaz [b,c], Rachid Salghi [c], Shehdeh Jodeh [d]

[a] Department of Chemistry, Deenbandhu Chhotu Ram University of Science and Technology, Murthal, Haryana, India
[b] Laboratory of separation processes, Faculty of Science, University Ibn Tofail PO Box 242, Kenitra, Morocco
[c] Laboratory of Applied Chemistry and Environment, ENSA, Ibn Zohr University, PO Box 1136, 80000 Agadir, Morocco
[d] Department of Chemistry, An-Najah National University, P. O. Box 7, Nablus, Palestine

ARTICLE INFO

Article history:
Received 10 June 2017
Received in revised form 7 August 2017
Accepted 11 August 2017
Available online 15 August 2017

Keywords:
Low Alloy Steel
Chromone
Corrosion
Inhibition efficiency, DFT

ABSTRACT

Chromone-3-acrylic acid (CA) and its derivatives viz. 6-hydroxy chromone-3-acrylic acid (6-OH-CA) and 7-methoxy chromone-3-acrylic acid (7-Me-CA) were synthesized and studied for inhibition of Low Alloy Steel corrosion in 1 M H_2SO_4 at different concentration and temperature using Gravimetric, Polarization technique, EIS, AFM, DFT and MD calculations. Mass loss, Potentiodynamic Polarization and EIS results showed that inhibition efficiency increased with gradual increments in concentration of CA compounds. Polarization study revealed that these compounds act as mixed type inhibitors and Langmuir adsorption isotherm is fitted well for adsorption. The order of inhibition efficiency is 7-Me-CA (88.00%) > CA (96.37%) > 6-OH-CA (96.77%). A proposed inhibition mechanism has further been described including the support from all the experimental as well as theoretical techniques.

1. Introduction

Low Alloy Steel (LAS) is commonly used as construction, storage and engineering material due to its cost affordability, abundance and convenience for fabrication. It also provides material properties that are acceptable for many applications in machinery and industry [1–3]. During oil well acidification as well as in oil recovery techniques in different acidic environments, gas production systems, rather, at every stage of production such as extraction, refining, storage and transportation of oil etc. through pipelines cause deterioration and sometimes, even failure of LAS equipments due to corrosion. Unfortunately, this corrosion of LAS leads to huge economic losses affecting badly any nation's GDP growth [4]. So, it demands crucially to develop some excellent and eco-friendly inhibitors, for, the most efficient and practical method to overcome corrosion is approached by implementing corrosion inhibitors in comparison to other corrosion controlling methods [5–7]. Moreover, the yield efficiency of inorganic corrosion inhibitors was found not so high in addition to their environmental risk [6–7].

The adsorption characteristics LAS of corrosion inhibitors depend upon the chemical moeity of the molecule, type of functional groups and the electron density at the donor atoms. Organic compounds, containing heteroatom's (N, O, S, and P), electronegative functional groups, π-electrons and aromatic rings as electron density rich centers which are considered as good adsorptive centers [8–9]. These heterocyclic organic inhibitors get adsorb onto the LAS surface or form protective insoluble layer and block corrosion sites, which reduces contact of corroding material with the corrosive medium/LAS [10].

Chromone and its derivatives make a class of naturally occurring heterocyclic compounds and have been isolated or synthesized for biological activities like anti-inflammatory, neuroprotective, anti-HIV, anti-tumor, anti-allergic, and, anti-cancer etc. [11–13]. Chromone class of compounds have not been much explored for corrosion control purposes except Bhkahk and Hadi who have reported corrosion inhibition studies of the Schiff bases of formyl chromones [14]. One of the interesting property of these compounds is their electron donating tendency towards metal ions, which enables them to form strong ligands in coordination compounds [15], thus, these compounds need to be explored in corrosion field also. In present study, we have chosen chromone-3-acrylic acid derivatives with oxygen as heteroatom along with π-electrons which may make them suitable agent for corrosion inhibition of LAS in sulphuric acid.

In view of this, three chromone compounds have been synthesized named as chromone-3-acrylic acid (CA), 6-hydroxy chromone-3-acrylic acid (6-OH-CA) and 7-methoxy chromone-3-acrylic acid (7-Me-CA) and studied their properties as corrosion inhibitors for LAS in 1 M sulphuric acid medium using various experimental techniques and theoretical aspects.

* Corresponding author.
E-mail address: sumanjakhar.chem@dcrustm.org (S. Lata).

http://dx.doi.org/10.1016/j.molliq.2017.08.048
0167-7322/

2. Experimental detail

2.1. Materials and sample preparation

The Low Alloy Steel, a rectangular sheet having composition (wt%); C = 0.14; Si = 0.03; Mn = 0.032; S = 0.05; P = 0.20; Ni = 0.01; Cu = 0.01; Cr = 0.01 and remainder iron (Fe) was used for all the experiments. The surface of LAS was abraded and polished mechanically with 400, 600, 800, 1000 and 2000 grade of emery paper (SiC). The working electrode was thereafter degreased with acetone, rinsed with bi-distilled water and then dried at room temperature before further use. The experiments were carried out at different temperatures (within ±0.1 °C accuracy) controlled thermostatically by using a water thermostat. The Chromone 3-Acrylic acid derivatives were synthesized as earlier reported [16–19] and the details of the characterization data for the synthesized inhibitors have been given in Supplementary Information. The chemical structures of the three acrylic acids are mentioned below:

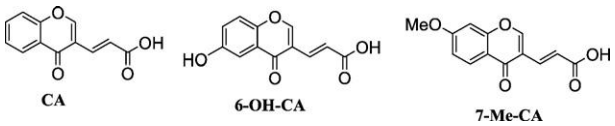

The acidic medium of 1 M H_2SO_4 was prepared by dilution analytical grade H_2SO_4 (minimum assay 98.0%, Qualikem, India) of known molarity with bidistilled water.

2.2. Experimental technique

2.2.1. Weight loss measurements

Weight loss experiments were conducted on finely abraded and polished and dried LAS sheets of dimension 3 × 1.5 × 0.028 cm^3 and weighing accurately using a digital balance (citizen scale CX 230) with 0.001 mg sensitivity. The Low Alloy Steel specimens were immersed in 1 M H_2SO_4 for 4 h in absence and presence of studied inhibitors at different temperature (303 K, 313 K, and 323 K,) and at different concentration (200, 400, 600, 800 and 1000 ppm). Once the weight loss experiments completed, the all specimens were cleaned with bidistilled water and acetone, dried and weighed again. All weight loss tests were carried out in triplicate with standard deviation of the order 0.01 for sample, not for population. The corrosion rate in mmpy was calculated from the Eq. (1)

$$\text{Corrosion rate } (CR) = \frac{534 \times \Delta W}{DAT} \tag{1}$$

where ΔW is the weight loss of LAS (mg), D is the density of Low Alloy Steel (7.86 g cm^{-3}), A is the total area of LAS sheet (cm^2), and T is the immersion time in hours. The CR values were used to calculate the inhibition efficiency (η) by the following equation.

$$\eta\% = \frac{CR^0 - CR}{CR^0} \times 100 \tag{2}$$

where CR and CR^0 are the values of corrosion rate of LAS with and without inhibitors, respectively.

2.3. Electrochemical measurements

Electrochemical measurements were conducted using electrochemical workstation PGSTAT204, Autolab, Netherland with FRA32M module controlled by NOVA 1.11 software. The electrochemical measurements were carried out using a three electrode cell assembly. A silver silver chloride electrode, provided with luggin capillary probe, was used as reference electrode along with graphite electrode as a counter electrode. The LAS acted as a working electrode (WE) with an exposed area of 1 cm^2, fitted to a specially designed holder and the tip of luggin probe was made in close proximity to working electrode in order to decrease the IR drop.

Before commencing the electrochemical measurements, the working electrode was kept for sufficient time in the corrosive solution which took 60 to 65 min in order to attain a constant value for the open circuit potential (OCP). Then, potentiodynamic polarization curve were recorded in absence and presence of the inhibitors in potential range from −250 to +250 mV with a scan rate of 0.001 V/s. Electrochemical parameters including cathodic and anodic Tafel slopes (β_c and β_a), corrosion potential (E_{corr}), corrosion rate (CR) and corrosion current density (i_{corr}) are placed in Table 2 at 303 K. The percentage inhibition efficiency was calculated using the relation:

$$\eta\% = \frac{i^0_{corr} - i_{corr}}{i^0_{corr}} \times 100 \tag{3}$$

where i^0_{corr} and i_{corr} are the corrosion current densities of LAS without and with inhibitor, respectively.

The Electrochemical Impedance Spectroscopy (EIS) measurement data were carried out from 100 kHz to 0.01 Hz using ac signal of 5 mV amplitude. EIS parameters include charge transfer resistance (R_{CT}), Constant Phase Element (CPE) and maximum frequency (f_{max}). Based on EIS data, the inhibition efficiency (η%), and double layer capacitance (C_{dl}) were calculated by using the following relation:

$$C_{dl=} \frac{1}{2\pi f_{max} R_{CT}} \tag{4}$$

$$\eta\% = \frac{R_{CT} - R^0_{CT}}{R^0_{CT}} \times 100 \tag{5}$$

where R_{CT} and R^0_{CT} are the values of charge transfer resistance with and without inhibitor, respectively.

2.4. Scanning electron microscopy (SEM)

LAS specimen were immersed in 1 M H_2SO_4 solution with and without inhibitors at 1000 ppm concentration for 4 h at 303 K after polishing and cleaning the LAS specimen by different grade of emery papers. Thereafter, the specimens retrieved, were washed with bidistilled water and dry acetone, dried and then kept in desiccator till they were transferred to SEM chamber for surface morphology. All the SEM images were taken at ×500 magnification.

2.5. Atomic force microscopy (AFM)

First, the samples were rubbed with SiC abrasive paper having range 600–2000 grade, followed by washing with bi-distilled water and acetone. After 4 h immersion in 1 M H_2SO_4 solution with and without inhibitor at room temperature, the specimens were cleaned with doubly distilled water and acetone and thereafter dried.

The topographic changes of the corroded metal surface of each specimen sheet having size 1 × 1 cm^2 were examined in standard mode with AFM Instrument (Model: Nanosurf Naio) from Molecular Image (Pico Scan). Micro-fabricated single beam Si_3N_4 having resonance frequency in the range of 13 kHz. The sparing constant (0.2 N/m) of the cantilevers was used to calculate the Roughness of Metal Surface (RMS) of the uninhibited and inhibited LAS and Nao program was used to interpret the image.

2.6. Molecular modeling detail

Density functional theory (DFT) method has been exploited for geometry optimizations and all quantum chemical parameters considering the system in water phase. Hybrid functional, B3LYP comprising

the Becke's three parameter exchange functional and Lee-Yang-Parr correlation functional in conjunction with 6-31G(d, p) basis set has been used for all the computation work. Gaussian09W software has been used for all the theoretical calculations [20–22]. Molecular Dynamic (MD) simulations of three studied inhibitors in this study have been carried out in a simulation box with periodic boundary conditions taking Materials Studio 6.0 (from Accelrys Inc.) [23]. The iron crystal was imported and cleaved along (110) plane and a slab of 5 Å was employed. The Fe (110) surface was relaxed by minimizing its energy with the help of smart minimizer method. Fe (110) surface was inflated to a (10 × 10) super cell in order to provide a large surface for the interaction of the acrylic acids. A vacuum slab with zero thickness was built. A supercell with a size of a = b = 24.82 Å c = 25.14 Å, consisting of 500 H_2O and molecules of tested inhibitors was created. The simulation was carried out in a simulation box (24.82 × 24.82 × 35.69 $Å^3$) using discover module with a time step of 1 fs and simulation time of 500 ps performed at 298 K, NVT ensemble, and COMPASS force field [24]. In simulation system, the interactions between Fe (110) and inhibitors can be understood by adsorption binding energies calculated using Eqs. (6) and (7) [25]:

$$E_{adsorption} = E_{total} - (E_{surface+solution} + E_{inhibitor+solution}) + E_{solution} \quad (6)$$

$$E_{binding} = -E_{adsorption} \quad (7)$$

where $E_{surface+solution}$ referred to the total energy of Fe (1 1 0) surface and solution without the inhibitors and $E_{inhibitor+solution}$ shows the total energy of inhibitors and solution; E_{total} gives the total energy of the entire system; and $E_{solution}$ is the total energy of the H_2O molecules.

3. Results and discussion

3.1. Weight loss measurements

3.1.1. Effect of concentration

It is clear from the weight loss data (Table 1) that the corrosion rate (*CR*) decreases and inhibition efficiency (η) increases with increase in concentration and reaching a maximum value, which is specific for each inhibitor. The relative strengths of inhibition capacity of the studied compounds at 303 K and 1000 ppm shows the order as CA (96.37%) ≈ 6-OH-CA (96.77%) > 7-Me-CA (88.00%).This trend may be due to the similarity of their molecular structures as well as the functional groups [26]. In absence of inhibitor, the corrosion rate is as high as 253.98 mmpy and with inhibitor at 303 K and 1000 ppm concentration, the *CR* values are reduced to 9.22 mmpy, 8.20 mmpy and 30.48 mmpy for CA, 6-OH-CA, and 7-Me-CA, respectively. Such findings indicate that all these compounds can be exploited as efficient corrosion inhibitors for LAS surface in 1 M H_2SO_4.

From the results shown in Table 1 at different temperature range (303 K, 313 K, and 323 K) in 1 M H_2SO_4 after 4 h immersion, it can be observed that I.E. % (η) value gets lessened as the temperature enhances from 303 K to 323 K and maximum inhibition efficiency was obtained at 303 K for all the three compounds.

3.1.2. Effect of temperature

In order to study the influence of temperature on % I.E. (η) of the investigated inhibitors, the weight loss experiments were carried out at different temperature i.e. (303 K, 313 K, and 323 K) after 4 h immersion in absence and presence of optimized concentration of the studied compounds are listed in Table 1. In corrosive medium, the elevated temperature frequently accelerates the metal dissolution rate of reaction and weakens the adsorption tendency of inhibitors on metallic surface. It can be seen from Table 1 that η value decreases at elevated temperature range from 303 K to 323 K and maximum inhibition efficiency was obtained at 303 K.

Also, the temperature dependency of corrosion rate can be represented by Arrhenius equation as

$$k_{corr} \; or \; log(CR) = -\frac{E_a}{2.303RT} + \log A \quad (8)$$

where k_{corr} is rate constant for corrosion reaction, log *CR* is the corrosion rate, E_a, apparent activation energy, *A* is the Arrhenius pre -exponential factor, *R* is universal gas constant and *T* is the absolute temperature.

Activation energy (E_a) data for all the inhibitors at 303 K and 1000 ppm concentration is determined from slope, equals to $-E_a$/2.303R from Eq. (8), and are listed in Table 2. The data indicate that values of activation energy are much higher in the presence of inhibitors 74.91 kJ mol^{-1} for 7-Me-CA, 121.43 kJ mol^{-1} for CA and for 6-OH-CA it is 127.65 kJ mol^{-1} in comparison to the value (42.35 kJ mol^{-1}) without inhibitor. These values highlighted that the energy barrier moves uphill for LAS dissolution in the presence of CA and derivatives resulting in reduced rate of corrosion process. Also, it is assumed that this increased activation energy is due to physical adsorption or electrostatic interaction between inhibitors and LAS surface occurring at the interface [27].

Table 1
CR and % inhibition efficiency (η) of CA, 6-OH-CA, and 7-Me-CA obtained from weight loss measurement in 1 M H_2SO_4 at various concentration and temperature.

Temperature		CA		6-OH-CA		7-Me-CA	
(K)	Concentration (ppm)	CR (mmpy)	η (%)	CR (mmpy)	η (%)	CR (mmpy)	η (%)
303	Blank	253.98	–	–	–	–	–
	200	41.11	83.81	37.56	85.21	55.16	78.28
	400	38.35	84.90	25.45	89.98	48.23	81.01
	600	27.96	88.99	14.40	94.33	44.44	82.50
	800	17.80	92.99	12.49	95.08	35.25	86.12
	1000	9.22	96.37	8.20	96.77	30.48	88.00
313	Blank	418.48	–	–	–	–	–
	200	133.54	68.09	121.86	70.88	167.06	60.08
	400	115.42	72.42	101.73	75.69	135.08	67.72
	600	100.81	75.91	83.70	80.00	129.08	69.00
	800	76.29	81.77	70.22	83.22	100.52	75.98
	1000	70.60	83.13	64.19	84.66	82.27	80.34
323	Blank	719.66	–	–	–	–	–
	200	325.86	54.72	309.38	57.01	344.86	52.08
	400	285.34	60.35	235.11	67.33	324.78	54.87
	600	223.81	68.90	226.76	68.49	292.75	59.32
	800	213.31	70.36	190.57	73.52	243.89	66.11
	1000	180.42	74.93	187.11	74.00	191.93	73.33

Table 2
Activation energy (E_a) of all CA derivatives.

Inhibitor	E_a (kJ mol^{-1})
Blank	42.35
CA	121.43
6-OH-CA	127.65
7-Me-CA	74.91

3.2. Electrochemical measurements

3.2.1. Potentiodynamic polarization measurement

Potentiodynamic polarization curves a, b and c show the Tafel parameters for CA, 6-OH-CA and 7-Me-CA respectively at 303 K as shown in Fig. 1 for LAS in 1 M H_2SO_4 solution in the absence and presence of different concentration of the inhibitors and the data obtained is given in Table 3. It is clearly seen from polarization curves that both cathodic and anodic curves shift to lower current densities on increasing the concentration of each inhibitor and shows the retardation of both hydrogen ion reduction as well as anodic dissolution reaction rates. This suppression of corrosion process can be attributed to adsorption on the metal surface through free electron pair from oxygen as well as π-electrons of each inhibitor and hence blocking the active sites of LAS surface [27]. The kinetic parameters of the corrosion reaction such as corrosion potential E_{corr} (mV), cathodic and anodic slopes β_a and β_c (mV/dec), corrosion current densities i_{corr} (μA cm^{-2}) and inhibition efficiency η (%) values are calculated from the Potentiodynamic polarization curves. Moreover, it is lucid that i_{corr} values decrease stridently in the presence of each inhibitor, which further lowers down gradually at higher concentration of each compound (Table 3).

According to Zarrouk, an inhibitor can be classified as anodic and cathodic type if the shift value in E_{corr} in the presence of inhibitor is >85 mV with respect to E_{corr} of blank [28–30] in either side and if the E_{corr} shift is <85 mV, it can be regarded as mixed type. But in case of all investigated CA derivatives, shifting in the value of E_{corr} is not >85 mV in either side with respect to the blank. This indicates that all CA derivatives act as mixed type inhibitor with predominant cathodic corrosion control.

3.2.2. EIS measurements

3.2.2.1. Electrochemical Impedance Spectroscopy (EIS). Nyquist plots in absence and presence of investigated inhibitors for LAS after around 60 to 65 min immersion (OCP value) in 1 M H_2SO_4 solution at 303 K are given in Fig. 3. Each impedance spectrum consists of one depressed capacitive semicircle at different concentration. Therefore, the equivalent circuit model shown in Fig. 2 was used to determine the EIS parameters and the results are listed in Table 4 which relates to electrical double layer behavior and strengthening the charge transfer process at the metal solution interface. The imperfect semicircle of Nyquist plots may also be attributed to surface roughness, frequency dispersion as well as heterogeneity of LAS surface [31]. Furthermore, the capacitive arc diameters in the presence of studied compounds are bigger than that observed in absence of inhibitor and this diameter broadens further with the increasing concentration of CA, 6-OH-CA and 7-Me-CA. Besides, similar shapes of all capacitive loops found in all cases, indicate that the difference of molecular structure of CA compounds may not affect the corrosion inhibition mechanism of LAS surface in 1 M H_2SO_4. This behavior suggests that the investigated inhibitors get adsorbed on LAS surface and block its active sites. Therefore, higher values for charge transfer resistance (R_{CT}) as well as inhibition efficiency are observed [32].

Where R_S (Ohm cm^2) = Solution resistance, R_p (Ohm cm^2) = Polarization resistance (also referred to as the charge transfer resistance), n = value of exponent of constant phase element. CPE = constant phase element.

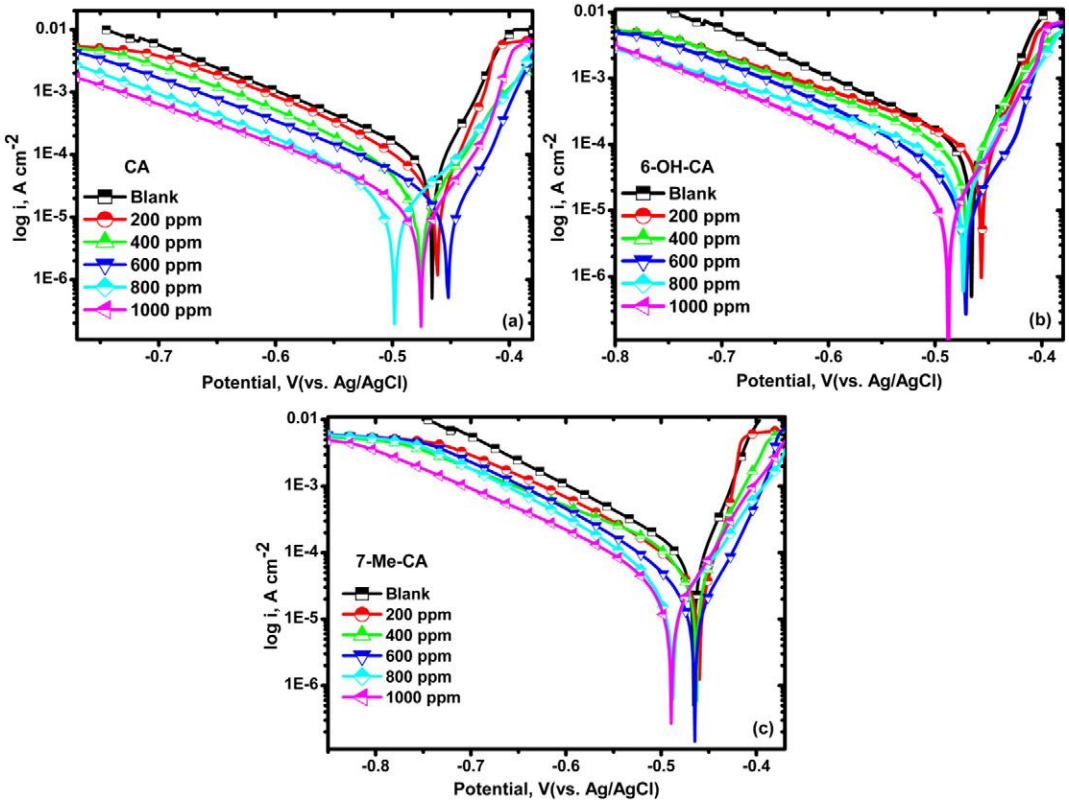

Fig. 1. Polarization curves of title compounds for LAS in 1 M H_2SO_4 at 303 K at different concentration.

Table 3
Potentiodynamic polarization parameters in absence and presence of CA and its derivatives at different concentration at 303 K.

Potentiodynamic Polarization parameters							
Inhibitor	C (ppm)	β_a (mV dec^{-1})	β_c (mV dec^{-1})	E_{corr}(mV vs. Ag/AgCl)	i_{corr} (μA cm^{-2})	η (%)	Θ
CA	Blank	150.63	37.58	466.0	146.46	–	–
	200	67.31	33.80	461.6	30.41	79.23	0.7923
	400	60.95	68.00	475.3	23.00	84.29	0.8429
	600	109.00	55.20	452.5	20.83	85.77	0.8577
	800	58.56	64.91	497.9	13.91	90.49	0.9049
	1000	33.75	48.70	475.6	5.01	96.57	0.9657
6-OH-CA	200	9.65	54.11	456.5	29.21	80.05	0.8005
	400	26.61	22.51	469.8	23.27	84.10	0.8410
	600	69.03	55.97	471.4	16.05	89.04	0.8904
	800	67.68	22.80	473.5	9.59	93.44	0.9344
	1000	17.96	16.35	487.6	2.74	98.12	0.9812
7-Me-CA	200	19.18	108.5	459.9	32.34	77.91	0.7791
	400	32.59	51.91	462.9	26.05	82.21	0.8221
	600	33.72	120.5	464.7	21.04	85.63	0.8563
	800	51.68	44.07	487.8	15.61	89.33	0.8933
	1000	41.34	63.84	489.3	10.73	92.67	0.9267

The fitted data from equivalent circuit such as R_{ct} (Ω cm^2), C_{dl} (μF cm^{-2}), f_{max} (Hz) and η of studied compounds are summarized in Table 4. R_{ct} and CPE are directly related with corrosion rate and formation of double layer at metal/solution interface. CPE suggests about the electrochemical behavior which is further related to the value of exponent n and n is often used to evaluate the impact of inhibitors adsorption. The value of n equivalent to 0, 0.5, 1 and −1 associated with the resistance, Warburg impedance, capacitance and inductance nature of surface, respectively. In the present work, the value n in most of the cases is nearer to 0.99 which is related to capacitance and the impedance way of CPE is defined as follows (Eq. (9)) [27]

$$Z_{CPE} = \left(\frac{1}{Y^{\circ}}\right)[(j\omega)_n]^{-1} \tag{9}$$

Typically, the addition of inhibitors give highest R_{ct} (314.57 Ω cm^2 for CA, 622.09 Ω cm^2 for 6-OH-CA and 199.51 Ω cm^2 for 7-Me-CA) have been found at 1000 ppm concentration while decreased C_{dl} value calculated by Eq. (4) with the concentration of inhibitors, suggesting the formation of a protective adsorption film on the LAS surface. The inhibition may be thought of due to the formation of inhibitive film over the LAS surface that gets more adhering by addition of more of inhibitor and hence showing the increase in charge transfer process mainly controlling the corrosion of LAS. Hence, decreased C_{dl} indicates the decrease in local dielectric constant and increase in double layer thickness which is due to adsorption of inhibitors at metal/solution interface [3,33]. In Figs. 1 and 2 of Supplementary Information show the Bode impedance and phase angle plots recorded for LAS electrode immersed in 1 M H_2SO_4 in the absence and presence of various concentration (200–1000 ppm) of studied inhibitors. Hence, the information provided by Bode Modulus and Phase angle diagrams strengthens the Nyquist behavior. Value of I.E. (η) increases with the concentration of inhibitors

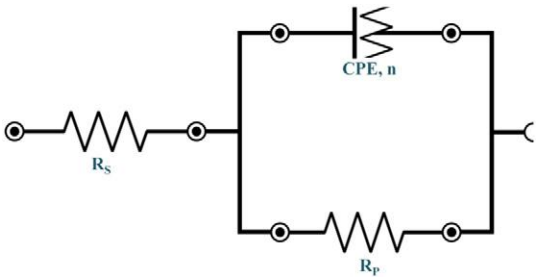

Fig. 2. Equivalent circuit model for all three studied inhibitors.

upto 95.26% for CA, 97.60% for 6-OH-CA and 92.42% for 7-Me-CA at 1000 ppm, in accordance with the results from potentiodynamic polarization as well as weight loss findings. However, the fact that the values are not in perfect agreement with each other might be due to the difference in testing techniques.

4. Adsorption isotherm and thermodynamic consideration

It is crucial to know about adsorption isotherm of LAS which can provide basic information about mechanism of corrosion inhibition for LAS due to the studied compounds. In order to characterize the adsorption behavior of inhibitors, various isotherms for LAS were employed such as Langmuir, Freundlich, Temkin, Flory-Huggins and Frumkin adsorption isotherm out of which, Langmuir adsorption isotherm gave the best description of adsorption behavior of investigated compounds [34]. The surface coverage (θ) is defined as given in Eq. (10)

$$\theta = \frac{\eta}{100} \tag{10}$$

where η is the inhibition efficiency observed from weight loss measurements. The results reveal that the plots of C/θ versus C offer ideal correlation coefficient ($R^2 \geq 0.99$) suitable which is given by Eq. (11) and in this study the surface coverage (θ) is obtained by Eq. (10).

$$\frac{C}{\theta} = \frac{1}{K_{ads}} + C \tag{11}$$

where θ is the extent of surface coverage and C is the concentration of studied inhibitors and K_{ads} is the equilibrium constant which can be calculated from the intercept of the plot of C/θ versus C (Fig. 4).

K_{ads} is related to the free energy of adsorption (ΔG°_{ads}) with the following Eq. (12).

$$K = \frac{1}{55.5}\ \exp\left(-\frac{\Delta G^{\circ}_{ads}}{RT}\right) \tag{12}$$

where T is absolute temperature, R is universal gas constant, and the value 55.5 (mol/L) is the concentration of water. According to Eq. (15), (ΔG°_{ads}) was calculated as −26.04 kJ mol^{-1}, −26.53 kJ mol^{-1} and −26.42 kJ mol^{-1} for CA, 6-OH-CA, and 7-Me-CA, respectively at 303 K (Table 5 and Fig. 4). The value of (ΔG°_{ads}) up to −20 kJ mol^{-1} are consistent with electrostatic interactions occurring between the charged inhibitor molecules and charged LAS surface (Physisorption) while those value around −40 kJ mol^{-1} or more negative involve formation of a coordinate type of bond between inhibitor molecules and LAS (chemisorption) [35–36]. The negative value of ΔG°_{ads} for inhibitors

Table 4
EIS parameters and inhibition efficiency value in the absence and presence of each title compounds.

Inhibitor	C (ppm)	R_{CT} (Ω cm^2)	C_{dl} (μF cm^{-2})	CPE		Chi Square	Θ	η %
				Y_0 (μF cm^{-2})	n			
Blank	–	14.909	380	293.25	0.99832	6.24×10^{-3}	–	–
CA	200	68.092	68.09	83.57	0.9984	3.51×10^{-3}	0.7810	78.10
	400	99.802	99.80	198.06	0.9985	4.09×10^{-3}	0.8506	85.06
	600	125.830	79.1	242.61	0.9989	5.47×10^{-3}	0.8815	88.15
	800	174.430	75.6	286.57	0.9985	5.30×10^{-3}	0.9145	91.45
	1000	314.570	55.6	265.85	0.9980	3.11×10^{-3}	0.9526	95.26
6-OH-CA	200	84.622	88.7	264.83	0.9974	1.98×10^{-3}	0.8238	82.38
	400	109.890	68.3	193.45	0.9988	3.86×10^{-3}	0.8643	86.43
	600	168.790	44.5	166.84	0.9989	4.55×10^{-3}	0.9116	91.16
	800	487.530	20.4	28.97	0.9985	1.63×10^{-3}	0.9694	96.94
	1000	622.090	16.0	163.21	0.9981	5.41×10^{-3}	0.9760	97.60
7-Me-CA	200	89.849	83.6	189.34	0.9989	4.31×10^{-3}	0.8340	83.40
	400	97.88	76.7	178.63	0.9983	5.12×10^{-3}	0.8476	84.76
	600	144.550	68.9	222.84	0.999	7.03×10^{-3}	0.8968	89.68
	800	196.730	66.1	156.64	0.999	1.08×10^{-2}	0.9242	92.42
	1000	199.510	50.6	231.49	0.997	7.69×10^{-3}	0.9252	92.52

CA, 6-OH-CA, and 7-Me-CA, indicate that the heterocyclic compounds can absorb on the LAS surface spontaneously with typical Physisorption (Table 5).

5. Scanning electron microscopy (SEM) study

The effect of inhibitors CA, 6-OH-CA, and 7-Me-CA on the surface morphology of the tested LAS was explored using SEM images of the corroded LAS surface in the absence and in the presence of inhibitors. Typical SEM photographs of the surfaces at ×500 magnification after immersion in 1 M H_2SO_4 at 303 K without and with 1000 ppm concentration for 4 h are shown in Fig. 5.The morphology in absence of each inhibitor reveals that the LAS surface is strongly corroded by acidic medium and resulting in a rough, porous and granular structure with corrosion products. In contrast, in the presence of each of the CA derivative, improvement in the LAS surface is observed resulting into smoother and crack free surface as observed in the micrographs b, c, and d. SEM observation clearly proves that all investigated compounds are quite effective corrosion inhibitors for LAS in the studied corrosive medium.

6. Atomic force microscopy (AFM)

The surface microstructure of the LAS in 1 M H_2SO_4 solution at 303 K before and after immersion and in the presence of all three inhibitors after 4 h of immersion was interpreted using AFM (Fig. 6). The rusted

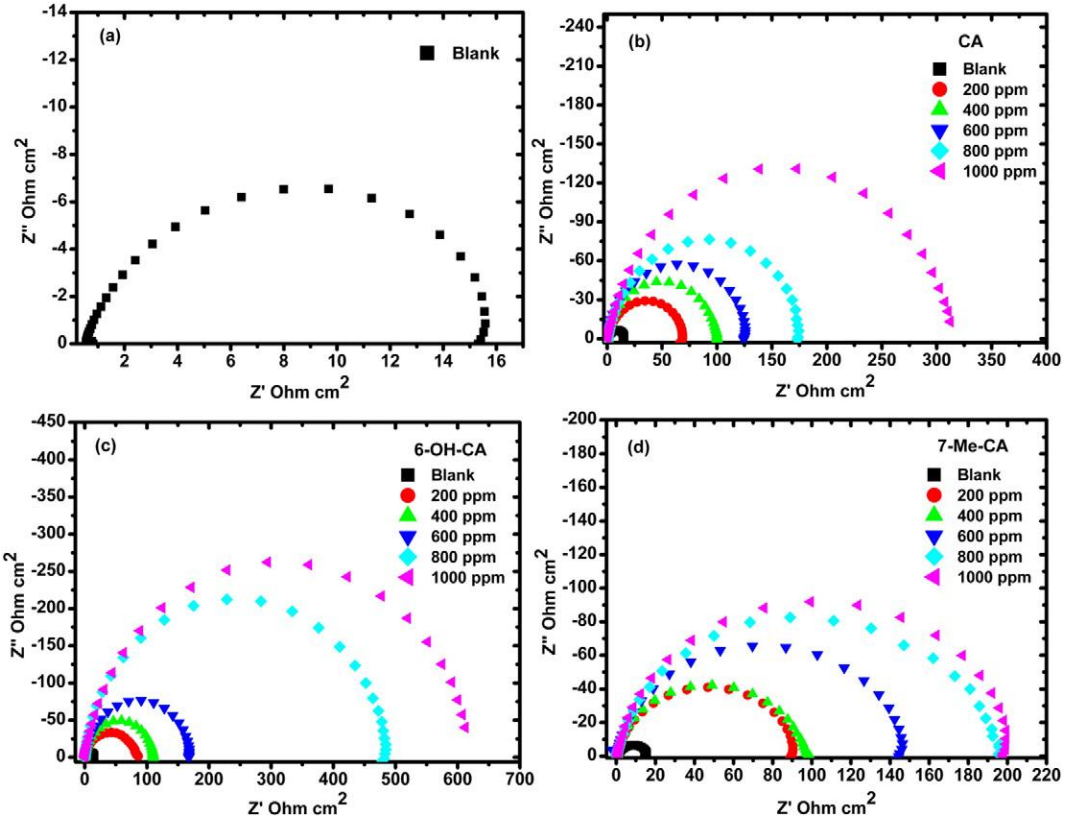

Fig. 3. Nyquist Plots for LAS in 1 M H_2SO_4 obtained at 303 K containing different concentration of title compounds.

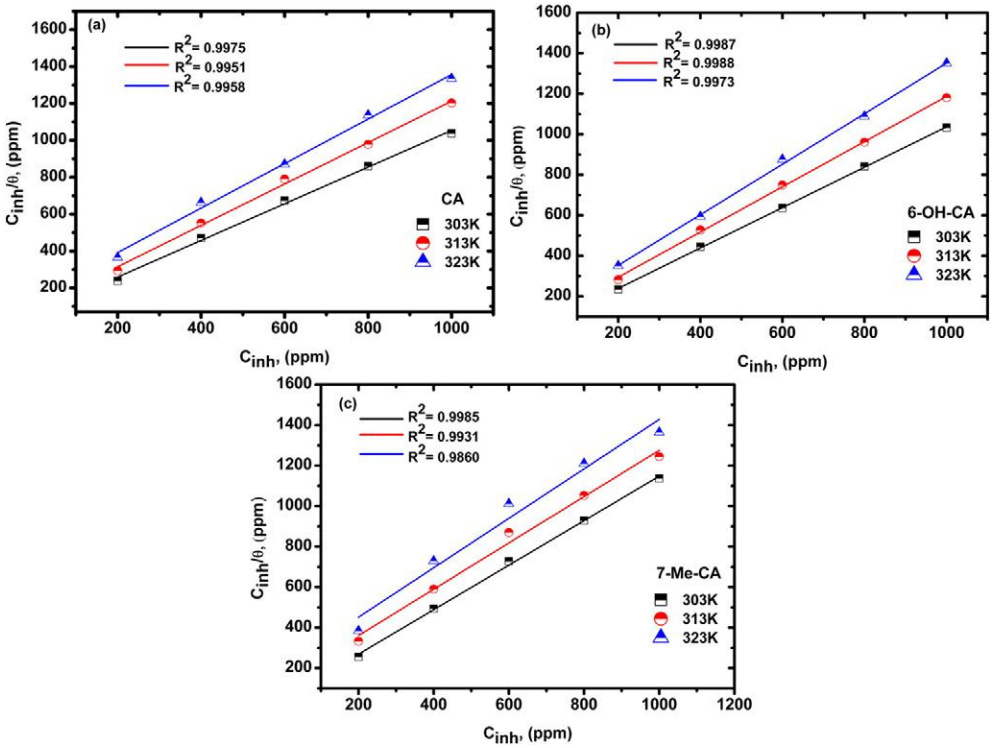

Fig. 4. Langmuir isotherm plots of title compounds for LAS in 1 M H_2SO_4 at different concentration and temperature.

surface in 1 M H_2SO_4 solution in the absence of Inhibitors looked relatively irregular, while it was relatively plane and compact in the presence of CA and its derivatives (Fig. 6) It is indisputably shown in Fig. 6 that the rusted surface in the presence of the CA derivatives were more uniform than the corroded one in the absence of inhibitor. The irregular and eroded LAS in 1 M H_2SO_4 solution without inhibitors

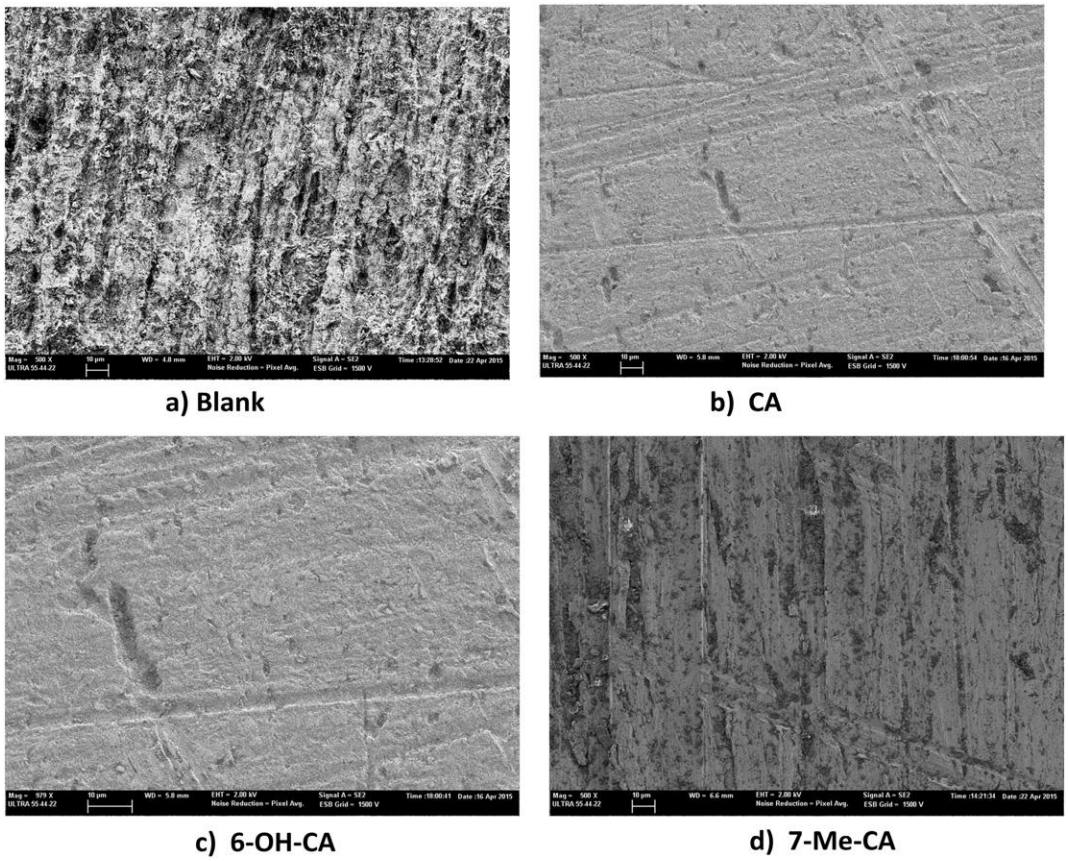

Fig. 5. Scanning Electron Micrographs of Blank and title compounds at 303 K and 1000 ppm.

indicated that the corrosion in this solution was usually electrochemical corrosion, while the more regular surface in the presence of CA and its derivatives suggested that all inhibitors in 1 M H_2SO_4 solution can form an adsorptive layer on the LAS surface that protects it from further more corrosion. An analyzed data in Fig. 6 revealed that the layer height values which indicate that the corrosion of steel decreases after adding CA and its derivatives in corrosive medium. In the presence of CA and its derivatives the corrosion rate were lower than those in the absence of all inhibitors. This was due to the formation of a layer of CA and its derivatives on the LAS surface, so the roughness of surface was very low. A comparison of Fig. 6 a, b, c, d and e clearly indicate that the corrosion of LAS reduced in the presence of CA and its derivatives and follows the following order of roughness of metal surface (RMS) 7-Me-CA > 6-OH-CA > CA (Table 6).

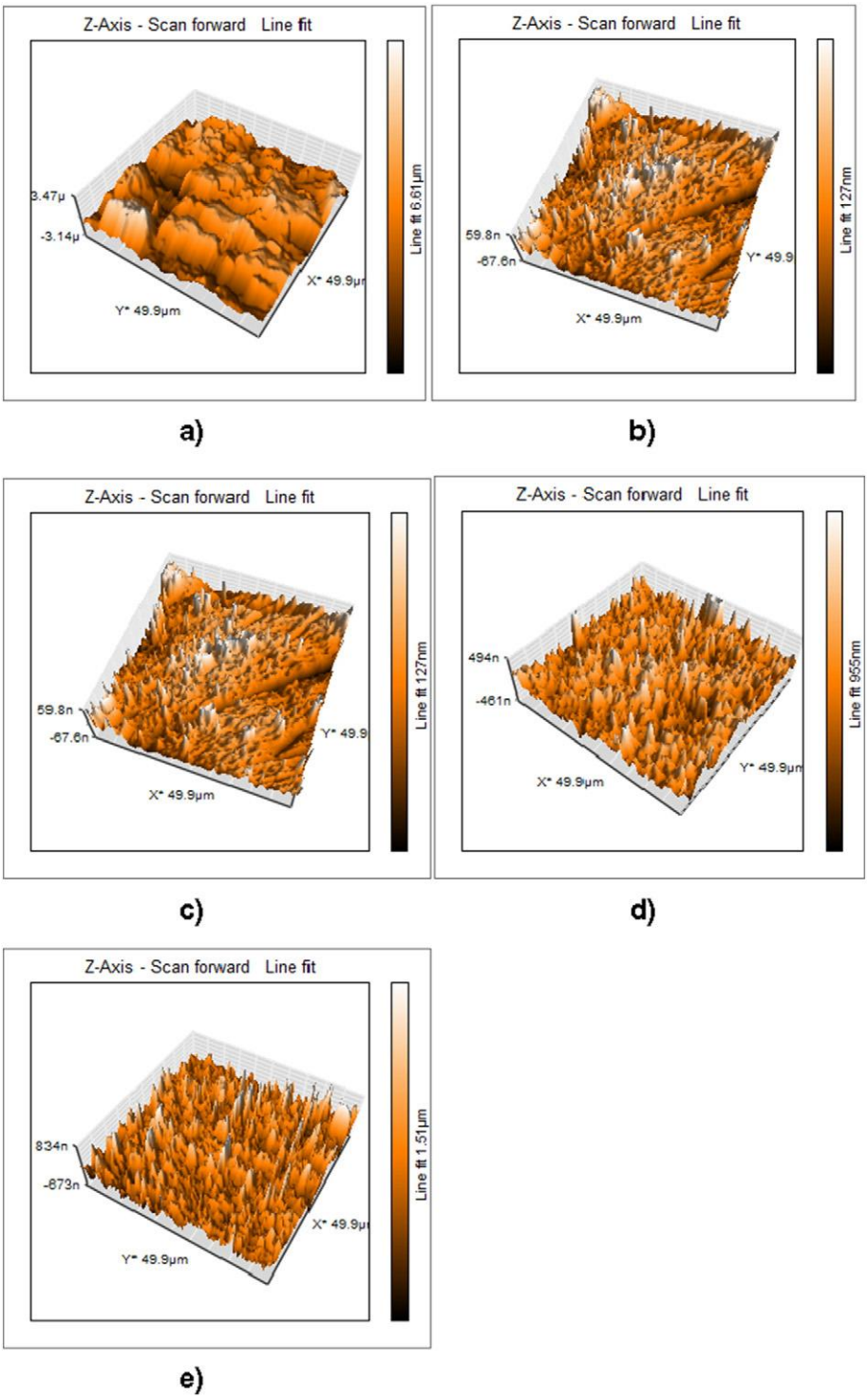

Fig. 6. Atomic force micrographs of LAS surfaces (a) AFM of LAS in 1 M H_2SO_4 (b) polished LAS (c) inhibited LAS (1 M H_2SO_4 + 1000 ppm CA) (d) inhibited LAS (1 M H_2SO_4 + 1000 ppm 6-OH-CA) and (e) inhibited LAS (1 M H_2SO_4 + 1000 ppm 7-Me-CA.)

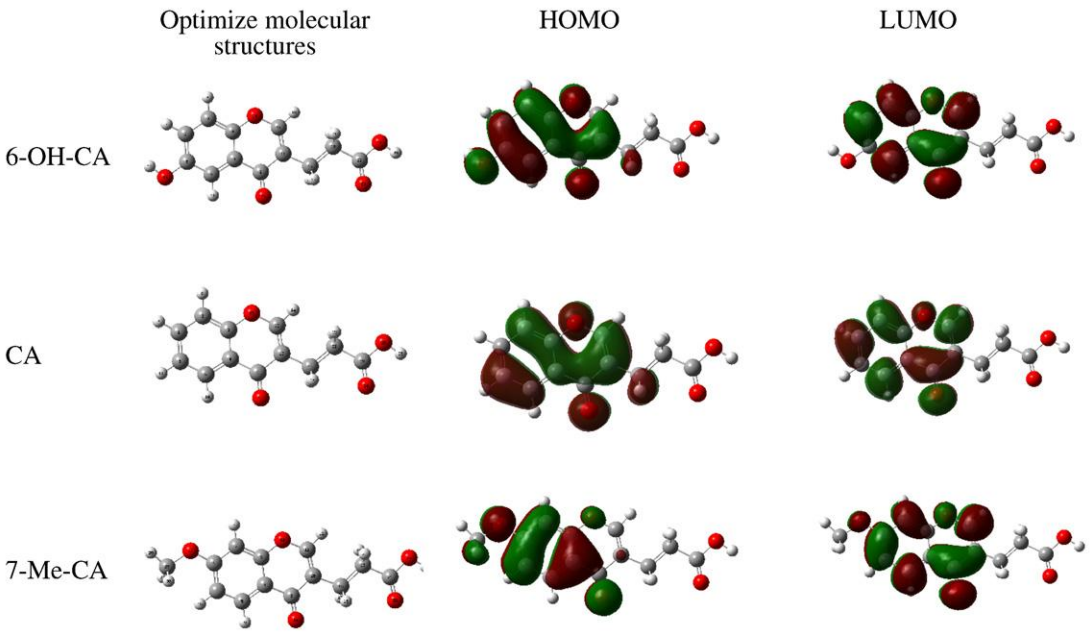

Fig. 7. DFT-derived geometry optimized structure, HOMO and LUMO plot of three molecules at B3LYP level in aqueous phase.

7. DFT calculations

Recently, the disposition of quantum chemical calculations in mentoring the corrosion inhibition mechanism has been substantially reported by Density Functional Theory (DFT) methods [37–38]. This type of study has also been considered as a powerful tool in gripping the interaction between the inhibitor and surface of the metal, which gives deep understanding about many complex interfacial phenomena at the molecular scale [39]. The highest occupied frontier molecular orbital (HOMO) and the lowest unoccupied frontier molecular orbital (LUMO) obtained as a result of the optimized molecular structure are represented in Fig. 7 in order to define the reactivity of an inhibitor. The HOMO frontier molecular electron distribution represents the electron donation as well as LUMO represents the electron acceptance ability of acrylic acids molecules [40,41]. It could be clearly seen from Fig. 7 that the HOMO and LUMO electrons are distributed over the entire molecule except in acetic acid parts, meaning the fine capability of the evaluated inhibitors to interact with the metal surface through donor-acceptor reactions.

The quantum chemical calculation parameters such as; E_{HOMO}, E_{LUMO}, ΔE and ΔN are placed in Table 6. The electron affinity (EA) and ionization potential (IP) are derived from E_{HOMO} and E_{LUMO} by the Eqs. (13) and (14):

$$IP = -E_{HOMO} \tag{13}$$

$$EA = -E_{LUMO} \tag{14}$$

Mulliken electronegativity (χ) and Absolute hardness (η) can be approximated as [42,43]:

$$\chi = \frac{IP + EA}{2} \tag{15}$$

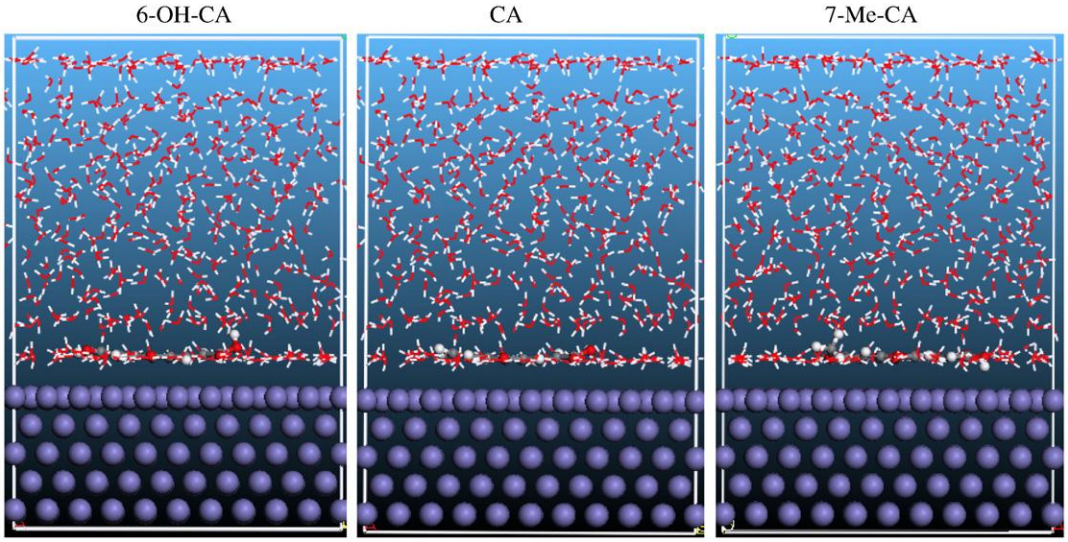

Fig. 8. Side view of the final adsorption of tested inhibitors on the Fe (1 1 0) surface in solution.

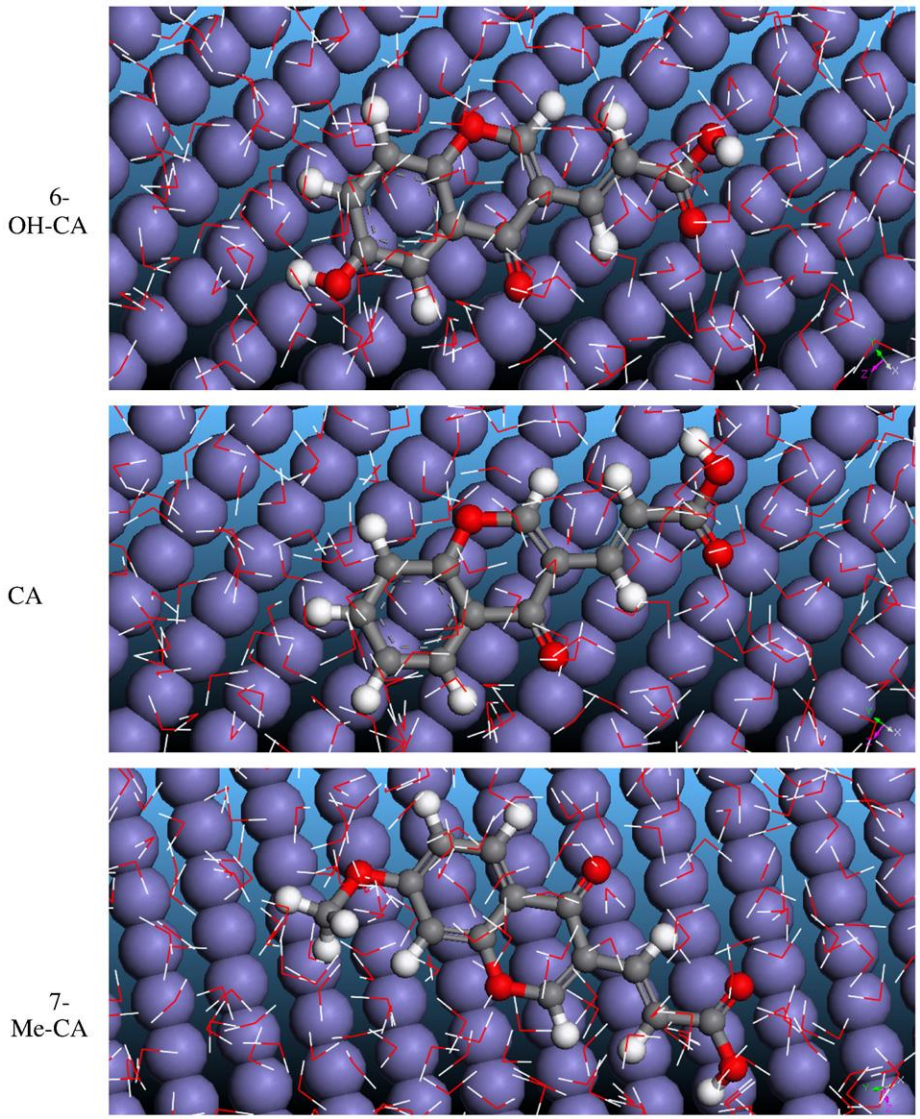

Fig. 9. Top view of the final adsorption of tested inhibitors on the Fe (1 1 0) surface in solution.

$$\eta = \frac{IP - EA}{2} \tag{16}$$

The number of transferred electrons (ΔN) has been calculated by application of the Pearson method using the Eq. (17) [44] as under

$$\Delta N = \frac{\chi_{Fe} - \chi_{inh}}{2(\eta_{Fe} + \eta_{inh})} \tag{17}$$

where χ_{Fe} and χ_{inh} denote the absolute electronegativity of iron and inhibitor molecule, η_{Fe} and η_{inh} represent the absolute hardness of iron and the inhibitor molecule respectively. A theoretical value of $\chi_{Fe} = 7$ eV and $\eta_{Fe} = 0$ (since for bulk metallic atoms, $I = A$) was considered in order to calculate the ΔN values [10,45–46]. Recently, it has been reported that the value of $\chi_{Fe} = 7$ eV is theoretically not acceptable since electron-electron interactions were not considered, rather, free electron gas Fermi energy of iron has been considered [47–49]. Hence, currently, the researchers are using work function (ϕ) of the metal surface instead of χ_{Fe}, as it is more appropriate parameter for its electronegativity value [49–51]. Thus, Eq. (18) is rewritten as follows:

$$\Delta N = \frac{\phi - \chi_{inh}}{2(\eta_{Fe} + \eta_{inh})} \tag{18}$$

Table 5
Thermodynamic parameters calculated from Langmuir adsorption isotherm for CA, 6-OH-CA, and 7-Me-CA in 1 M H_2SO_4 at 303 K, 313 K, and 323 K.

Temperature (K)	CA		6-OH-CA		7-Me-CA	
	$1/K_{ads}$ (M)	ΔG°_{ads}	$1/K_{ads}$ (M)	ΔG°_{ads}	$1/K_{ads}$ (M)	ΔG°_{ads}
303	44.05	26.04	36.28	26.53	37.90	26.42
313	80.71	25.32	65.74	25.86	101.76	24.72
323	128.39	24.8	128.39	24.89	143.47	24.59

Table 6
Parameter for roughness of metal surface (RMS).

Sr. no.	Inhibitors	RMS value
1	Blank	729.41
2	Plain	45.51
3	CA	71.277
4	6-OH-CA	118.77
5	7-Me-CA	147.68

Table 7
The computed quantum chemical parameters for tested compounds.

Inhibitor	E_{HOMO} (eV)	E_{LUMO} (eV)	ΔE_{gap} (eV)	ΔN_{110}
6-OH-CA	−6.049	−1.534	4.514	0.227
CA	−6.476	−1.529	4.947	0.165
7-Me-CA	−6.378	−1.349	5.028	0.190

The observed DFT derived ϕ value for Fe (1 1 0) surface is 4.82 eV [47–48]. According to Frontier Molecular Orbital (FMO) theory, an inhibitor with high E_{HOMO} energy value is associated with strong electron donating ability and therefore with better inhibition efficiency [51–52]. Opposite to E_{HOMO}, low E_{LUMO} energy of a molecule indicates its ability to accept electrons from the metallic surface and hence higher inhibition efficiency. Accordingly, the difference between HOMO and LUMO energies known as energy gap is another important parameter which provides conclusive information about the stability index of the corrosion inhibitor. The lower the orbital energy gap (ΔE), the higher is the interaction between inhibitor and metal surface [53–54]. As is shown in Table 7, the E_{LUMO} decreases in the order of 7-Me-CA > CA >6-OH-CA, indicating that the inhibitors accept electrons from the surface of metal following the order 6-OH-CA > CA >7-Me-CA. Moreover, the energy band gap values also get decreased in the order of 7-Me-CA > CA >6-OH-CA, demonstrating that the stability of the formed complex on the metal surface follows the order of 6-OH-CA > CA >7-Me-CA which lucidly explore the high inhibition efficiency observed in the case of 6-OH-CA as compared to that of CA and 7-Me-CA. Analysis of the results shown in Table 7 indicates that the order of HOMO energies does not obey the order of inhibition efficiencies, this result is often interpreted by the presence of complex interactions between inhibitors and the metal surface. It has also been reported that the ΔN value gives a measure of the ability of a chemical compound to transfer its electrons towards metal if $\Delta N > 0$ and vice versa if $\Delta N < 0$ [55–57]. In the present study, the positive values of ΔN represented in Table 7, suggest that the high capability of studied inhibitors donates electrons to the LAS surface. We have cited in the experimental part that the tested inhibitors get adsorbed on the metal surface primarily by physical interactions, which means that the inhibitors often accept electrons from the metal surface, this inference is easy to be understood considering that our compounds contain many oxygen atoms that easily get protonated in the acid medium, whereas, the double bonds existing in the acrylic acids are most probably, the origin of chemical interactions. The findings of theoretical calculation are very well compatible with those obtained through the experimental results.

7.1. Molecular dynamic (MD) simulations

Additionally, in order to understand the adsorption behavior of the studied inhibitors, MD simulations have been carried out in the system consisting of the inhibitor molecules and water molecules. The binding and interaction energies of the adsorbed inhibitors have been approximated when the simulation system reached their equilibrium state. The best adorable adsorption configuration of the studied molecules on Fe (110) surface is shown in Figs. 8 and 9 while the interaction and binding energies are placed in Table 8.

It is noticeable that all the three inhibitors adopt near-flat orientation on the surface of Fe (110). This parallel adsorption supports optimized interactions with a metallic surface. The presence of π-electrons as well as the sufficient amount of oxygen atoms in the molecular structure of our compounds can facilitate donor-acceptor interactions which allows the inhibitor molecules to provide larger blocking area preventing the LAS surface from corrosion attack.

Table 8
Selected energy parameters obtained from MD simulations for adsorption of the inhibitors on Fe (110) surface.

System	$E_{Interaction}$ (kJ mol^{-1})	$E_{Binding}$ (kJ mol^{-1})
Fe + 6-OH-CA/500H_2O	−520,16	520,16
Fe + CA/500H_2O	−411,07	411,07
Fe + 7-Me-CA/500H_2O	−389,03	389,03

The results shown in Table 7 clarify that the 6-OH-CA has a better adsorption capability as compared to the other two compounds (CA and 7-Me-CA). The high negative energy suggests the strong and stable adsorption of the inhibitors on Fe (110) surface [57–58]. It can also be observed that the binding energy of 6-OH-CA is far higher than that of CA and subsequently 7-Me-CA, hence, has the less adsorption efficiency [59–60]. These results are in good accordance with the experimentally obtained inhibition efficiency as well as the results obtained from DFT calculations.

8. Conclusion

The synthesized compounds i.e. chromone-3-acrylic acid (CA), 6-hydroxy chromone-3-acrylic acid (6-OH-CA) and 7-methoxy chromone-3-acrylic acid (7-Me-CA) are tested for the first time as corrosion inhibitors for control of corrosion of Low Alloy Steel (LAS) in 1 M H_2SO_4 and showed great inhibition efficiency. Further, the values of inhibition efficiency of the three acrylic acids get enhanced with increase in their concentration and reduced at the elevated temperatures. The potentiodynamic polarization curves have shown that the synthesized compounds acted as mixed type inhibitors. The results of gravimetric analysis, Potentiodynamic polarization, and EIS are found to be in very good agreement with the theoretical aspects. Adsorption isotherms showed that all the three inhibitors obey Langmuir adsorption isotherm and free energy (ΔG) values suggest the physical adsorption aided by slight chemical type adsorption, as the controlling factor for the inhibition process. Furthermore, DFT calculations and MD simulations comfortably agree with the experimental data revealing that the inhibitors get effectively adsorbed on the surface of LAS in planar manner. SEM and AFM studies also strengthen all the findings.

Acknowledgement

The authors are grateful to University Grants Commission (UGC) under Major Research Project vide file no. 42-292/2013(SR) dated April, 2013 and Dept. of Chemistry, Deenbandhu Chhotu Ram University of Science and Technology, Murthal, Sonipat, Haryana for financial assistance.

Appendix A. Supplementary data

Supplementary data to this article can be found online at http://dx.doi.org/10.1016/j.molliq.2017.08.048.

References

[1] Z. El Adnani, M. Mcharfi, M. Sfaira, M. Benzakour, A.T. Benjelloun, M.E. Touhami, DFT theoretical study of 7-R-3methylquinoxalin-2(1H)-thiones (R=H; CH_3; Cl) as corrosion inhibitors in hydrochloric acid, Corros. Sci. 68 (2013) 223–230.
[2] A. Zarrouk, B. Hammouti, T. Lakhlifi, M. Traisnel, H. Vezin, F. Bentiss, New 1H-pyrrole-2,5-dione derivatives as efficient organic inhibitors of carbon steel corrosion in hydrochloric acid medium: electrochemical, XPS and DFT studies, Corros. Sci. 90 (2015) 572–584.
[3] S. Dahiya, S. Lata, R. Kumar, O. Yadav, Comparative performance of Uroniums for controlling corrosion of steel with methodical mechanism of inhibition in acidic medium: part 1, J. Mol. Liq. 221 (2016) 124–132.
[4] R.A. Prabhu, T.V. Venkatesha, A.V. Shanbhag, Quinol-2-thione compounds as corrosion inhibitors for mild steel in acid solution, Mater. Chem. Phys. 108 (2008) 283–289.
[5] H. Lgaz, S. Rachid, M. Larouj, M. Elfaydy, S. Jodeh, H. Abbout, B. Lakhrissi, K. Toumiat, H. Oudda, Moroc. J. Chem. Mor. 4 (2016) 592.
[6] G. Khan, K.Md.S. Newaz, W.J. Basirun, H.B.M. Ali, F.L. Faraj, G.M. Khan, Application of natural product extracts as green corrosion inhibitors for metals and alloys in acid pickling processes-A, Int. J. Electrochem. Sci. 10 (2015) 6120–6134.
[7] G. Khan, W.J. Basirun, S.N. Kazi, P. Ahmed, L. Magaji, S.M. Ahmed, G.M. Khan, M.A. Rehman, Electrochemical investigation on the corrosion inhibition of mild steel by

Quinazoline Schiff base compounds in hydrochloric acid solution, J. Colloid Interface Sci. 502 (2017) 134–145.
[8] J.I. Bregman, Corrosion Inhibitors, Macmillan Co., New York, 1963.
[9] K. Bhrara, G. Singh, The inhibition of corrosion of mild steel in 0.5 M sulfuric acid solution in the presence of benzyl triphenyl phosphonium bromide, Appl. Surf. Sci. 253 (2006) 846–853.
[10] R. Kumar, S. Chahal, S. Dahiya, N. Dahiya, S. Kumar, S. Lata, Experimental and theoretical approach to exploit the corrosion inhibition activity of 3-formylchromone derivatives on mild steel in 1 m H_2SO_4, Corros. Rev. 35 (2) (2017) 111–121.
[11] N.S. Joshi, B.K. Karale, C.H. Gill, S.B. Bhirud, Synthesis and characterization of new biologically active 2-(1, 3-disubstituted pyrazolyl) chromones and corresponding pyrimidine, thiopyrimidine, pyrazolyl derivatives, J. Heterocycl. Chem. 41 (4) (2004) 541–548.
[12] M. Kawase, T. Tanaka, H. Kan, S. Tani, H. Nakashima, H. Sakagami, Biological activity of 3-formylchromones and related compounds, In Vivo 21 (2007) 829–834.
[13] N.R. Guz, F.R. Stermitz, J.B. Johnson, T.D. Beeson, S. Willen, J.F. Hsiang, K. Lewis, Flavonolignan and flavone. Inhibitors of a *Staphylococcus aureus* multidrug resistance pump: structure–activity relationships, J. Med. Chem. 44 (2001) 261–268.
[14] C.K. Bhkahk, J.S. Hadi, New unsymmetrical Schiff base as inhibitor of carbon steel corrosion and antibacterial activity, Res. J. Chem. Sci. 5 (1) (2015) 64–70.
[15] N.H. Kolhe, S.S. Jadhav, S.J. Takate, A.E. Athare, S.P. Salve, Synthesis, characterization and biological screening of Cu (II)-3-formylchromone derivative complex, J. Appl. Chem. 7 (2014) 26–32.
[16] A. Nohara, T. Umetani, Y. Sanno, Studies on antianaphylactic agents—I: a facile synthesis of 4-oxo-4H-1-benzopyran-3-carboxaldehydes by Vilsmeier reagents, Tetrahedron 30 (1974) 3553–3561.
[17] B.S. Furniss, A.J. Hannaford, B. Rogers, P.W.G. Smith, A.R. Tatchell, Vogel's Textbook of Practical Organic Chemistry, 5th ed. Harlow: Longman, 1989 751.
[18] K. Chand, R.K. Tiwari, S. Kumar, N. Amir Shirazi, S. Sharma, E.V. Eycken, V.S. Parmar, K. Parang, S.K. Sharma, Synthesis. Antiproliferative, and c-Src kinase inhibitory activities of 4-oxo-4H-1-benzopyran derivatives, J. Heterocycl. Chem. 52 (2015) 562.
[19] V.K. Ahluwalia, B.P. Arrarwal, R. Chandra, Intermediates for Organic Synthesis, IK International Pvt Ltd, 2005 118.
[20] A.D. Becke, Density-functional exchange-energy approximation with correct asymptotic behavior, Phys. Rev. A 38 (1988) 3098–3100, http://dx.doi.org/10.1103/PhysRevA.38.3098.
[21] C. Lee, W. Yang, R.G. Parr, Development of the Colle-Salvetti correlation-energy formula into a functional of the electron density, Phys. Rev. B 37 (1988) 785–789, http://dx.doi.org/10.1103/PhysRevB.37.785.
[22] M. Frisch, G. Trucks, H. Schlegel, G. Scuseria, M. Robb, J. Cheeseman, G. Scalmani, V. Barone, B. Mennucci, G. Petersson, 01, Gaussian, Inc, Wallingford CT, 2009.
[23] B. Ime, Metronidazole as Environmentally Safe Corrosion Inhibitor for Mild Steel in 0.5 M HCl: Experimental and Theoretical Investigation. Materials Studio, Revision 6.0, vol. 1 (3), Accelrys Inc., San Diego, USA, 2013 (491–439).
[24] H. Sun, COMPASS: an ab initio force-field optimized for condensed-phase applications overview with details on alkane and benzene compounds, J. Phys. Chem. B 102 (1988) 7338–7364.
[25] Z. Zhang, N.C. Tian, X.D. Huang, W. Shang, L. Wu, Synergistic inhibition of carbon steel corrosion in 0.5 M HCl solution by indigo carmine and some cationic organic compounds: experimental and theoretical studies, RSC Adv. 6 (2016) 22250–22268, http://dx.doi.org/10.1039/C5RA25359D.
[26] E.E. Ebenso, M.M. Kabanda, L.C. Murulana, A.K. Singh, S.K. Shukla, Electrochemical and quantum chemical investigation of some azine and thiazine dyes as potential corrosion inhibitors for mild steel in hydrochloric acid solution, Ind. Eng. Chem. Res. 51 (2012) 12940–12958.
[27] C. Verma, M.A. Quraishi, L.O. Olasunkanmi, E.E. Ebenso, L-Proline-promoted synthesis of 2-amino-4-arylquinoline-3-carbonitriles as sustainable corrosion inhibitors for mild steel in 1 M HCl: experimental and computational studies, RSC Adv. 5 (2015) 85417.
[28] A. Zarrouk, B. Hammouti, T. Lakhlifi, New 1H-pyrrole-2,5-dione derivatives as efficient organic inhibitors of carbon steel corrosion in hydrochloric acid medium: electrochemical, XPS and DFT studies, Corros. Sci. 90 (2015) 572–584.
[29] K.G. Zhang, B. Xu, W.Z. Yang, Halogen-substituted imidazoline derivatives as corrosion inhibitors for mild steel in hydrochloric acid solution, Corros. Sci. 90 (2015) 284–295.
[30] X. Leia, H. Wang, Y. Fengc, J. Zhanga, X. Suncd, S. Laib, Z. Wangb, S. Kangb, Synthesis, evaluation and thermodynamics of a 1H-benzoimidazole phenanthroline derivative as a novel inhibitor for mild steel against acidic corrosion, RSC Adv. 00 (2015) 1–11.
[31] B. Xu, Y. Ji, X. Zhang, X. Jin, W. Yang, Y. Chen, Experimental and theoretical studies on the corrosion inhibition performance of 4-amino-N,N-di-(2-pyridylmethyl)-aniline on mild steel in hydrochloric acid, RSC Adv. 5 (2015) 56049–56059.
[32] P. Roy, P. Karfa, U. Adhikari, D. Sukul, Corrosion inhibition of mild steel in acidic medium by polyacrylamide grafted Guar gum with various grafting percentage: effect of intramolecular synergism, Corros. Sci. 88 (2014) 246–253.
[33] K.F. Khaled, N. Hackerman, Mater. Chem. Phys. 82 (2003) 949–960.
[34] C.J. Zou, X.L. Yan, Y.B. Qin, Inhibiting evaluation of β-cyclodextrin-modified acrylamide polymer on alloy steel in sulfuric solution, Corros. Sci. 85 (2014) 445–454.
[35] C. Verma, M.A. Quraishi, E.E. Ebenso, I.B. Obot, A. El. Assyry, 3-Amino alkylated indoles as corrosion inhibitors for mild steel in 1 M HCl: experimental and theoretical studies, J. Mol. Liq. 219 (2016) 647.
[36] Q. Qu, Z.Z. Hao, L. Li, Synthesis and evaluation of tris-hydroxymethyl-(2-hydroxybenzylidenamino)-methane as a corrosion inhibitor for cold rolled steel in hydrochloric acid, Corros. Sci. 51 (2009) 569–574.
[37] R.N. Singh, A. Kumar, R.K. Tiwari, P. Rawat, A combined experimental and theoretical (DFT and AIM) studies on synthesis, molecular structure, spectroscopic properties and multiple interactions analysis in a novel ethyl-4-[2-(thiocarbamoyl)hydrazinylidene]-3,5-dimethyl-1H-pyrrole-2-carboxylate and its dimer, Spectrochim. Acta A Mol. Biomol. Spectrosc. 112 (2013) 182–190, http://dx.doi.org/10.1016/j.saa.2013.04.002.
[38] H. Jafari, I. Danaee, H. Eskandari, M. RashvandAvei, Combined computational and experimental study on the adsorption and inhibition effects of N_2O_2 Schiff base on the corrosion of API 5L grade B steel in 1 mol/L HCl, J. Mater. Sci. Technol. 30 (2014) 239–252, http://dx.doi.org/10.1016/j.jCSt.2014.01.003.
[39] S.K. Saha, P. Ghosh, A. Hens, N.C. Murmu, P. Banerjee, Density functional theory and molecular dynamic simulation study on corrosion inhibition performance of mild steel by mercapto-quinoline Schiff base corrosion inhibitor, Phys. E Low-Dimens. Syst. Nanostruct. 66 (2015) 332–341, http://dx.doi.org/10.1016/j.physe.2014.10.035.
[40] M. Yadav, R.R. Sinha, T.K. Sarkar, N. Tiwari, Corrosion inhibition effect of pyrazole derivatives on mild steel in hydrochloric acid solution, J. Adhes. Sci. Technol. 29 (2015) 1690–1713.
[41] H. Lgaz, R. Salghi, S. Jodeh, B. Hammouti, Effect of clozapine on inhibition of Mild Steel corrosion in 1.0 M HCl medium, J. Mol. Liq. 225 (2017) 271–280.
[42] R.G. Pearson, Absolute electronegativity and hardness: application to inorganic chemistry, Inorg. Chem. 27 (1988) 734–740.
[43] V. Sastri, J. Perumareddi, Molecular orbital theoretical studies of some organic corrosion inhibitors, Corrosion 53 (1997) 617–622.
[44] S. Martinez, Inhibitory mechanism of mimosa tannin using molecular modeling and substitutional adsorption isotherm, Mater. Chem. Phys. 77 (2003) 97–102.
[45] A.Y. Musa, A.A.H. Kadhum, A.B. Mohamad, M.S. Takriff, Molecular dynamics and quantum chemical calculation studies on 4, 4-dimethyl-3-thiosemicarbazide as corrosion inhibitor in 2.5 M H_2SO_4, Mater. Chem. Phys. 129 (2011) 660–665.
[46] H. Shokry, Molecular dynamics simulation and quantum chemical calculations for the adsorption of some Azo-azomethine derivatives on mild steel, J. Mol. Struct. 1060 (2014) 80–87.
[47] Z. Cao, Y. Tang, H. Cang, J. Xu, G. Lu, W. Jing, Novel benzimidazole derivatives as corrosion inhibitors of mild steel in the acidic media. Part II: theoretical studies, Corros. Sci. 83 (2014) 292–298.
[48] A. Kokalji, On the HSAB based estimate of charge transfer between adsorbates and metal surfaces, Chem. Phys. 393 (2012) 1–12.
[49] I. Obot, D. Macdonald, Z. Gasem, Density functional theory (DFT) as a powerful tool for designing new organic corrosion inhibitors. Part 1: an overview, Corros. Sci. 99 (2015) 1–30.
[50] H. Lgaz, R. Salghi, M. Larouj, M. Elfaydy, S. Jodeh, Z. Rouifi, B. Lakhrissi, H. Oudda, Experimental, theoretical and Monte Carlo simulation of quinoline derivative as effective corrosion inhibitor for mild steel in 1 M HCl, J. Mater. Environ. Sci. 7 (2016) 4471–4488.
[51] A.O. Yüce, E. Telli, B.D. Mert, G. Kardaş, B. Yazıcı, Experimental and quantum chemical studies on corrosion inhibition effect of 5,5 diphenyl 2-thiohydantoin on mild steel in HCl solution, J. Mol. Liq. 218 (2016) 384–392, http://dx.doi.org/10.1016/j.molliq.2016.02.087.
[52] S. Kumar, D. Sharma, P. Yadav, M. Yadav, Experimental and quantum chemical studies on corrosion inhibition effect of synthesized organic compounds on N80 steel in hydrochloric acid, Ind. Eng. Chem. Res. 52 (2013) 14019–14029, http://dx.doi.org/10.1021/ie401308v.
[53] Y. El Aoufir, H. Lgaz, H. Bourazmi, Y. Kerroum, Y. Ramli, A. Guenbour, R. Salghi, F. El-Hajjaji, B. Hammouti, H. Oudda, Quinoxaline derivatives as corrosion inhibitors of carbon steel in hydrochloridric acid media: electrochemical, DFT and Monte Carlo simulations studies, J. Mater. Environ. Sci. 7 (2016) 4330–4347.
[54] S.K. Saha, A. Dutta, P. Ghosh, D. Sukul, P. Banerjee, Novel Schiff base molecules as efficient corrosion inhibitors for mild steel surface in 1 M HCl medium: experimental and theoretical approach, Phys. Chem. Chem. Phys. 18 (2016) 17898–17911.
[55] A. Kokalj, Is the analysis of molecular electronic structure of corrosion inhibitors sufficient to predict the trend of their inhibition performance, Electrochim. Acta 56 (2010) 745–755.
[56] N. Kovačević, A. Kokalj, Analysis of molecular electronic structure of imidazole-and benzimidazole-based inhibitors: a simple recipe for qualitative estimation of chemical hardness, Corros. Sci. 53 (2011) 909–921.
[57] S.-W. Xie, Z. Liu, G.-C. Han, W. Li, J. Liu, Z. Chen, Molecular dynamics simulation of inhibition mechanism of 3, 5-dibromo salicylaldehyde Schiff's base, Comput. Theor. Chem. 1063 (2015) 50–62.
[58] Z. Zhang, N. Tian, X. Li, L. Zhang, L. Wu, Y. Huang, Synergistic inhibition behavior between indigo carmine and cetyl trimethyl ammonium bromide on carbon steel corroded in a 0.5 M HCl solution, Appl. Surf. Sci. 357 (Part A) (2015) 845–855, http://dx.doi.org/10.1016/j.apsusc.2015.09.092.
[59] Z. Zhang, N.C. Tian, X.D. Huang, W. Shang, L. Wu, Synergistic inhibition of carbon steeel corrosion in 0.5 M HCl solution by indigo carmine and some cationic organic compounds: experimental and theoretical studies, RSC Adv. 6 (2016) 22250–22268, http://dx.doi.org/10.1039/C5RA25359D.
[60] S.-W. Xie, Z. Liu, G.-C. Han, W. Li, J. Liu, Z. Chen, Molecular dynamics simulation of inhibition mechanism of 3, 5-dibromo salicylaldehyde Schiff's base, Comput. Theor. Chem. 1063 (2015) 50–62.